Suppression of superconductivity dominated by proximity effect in amorphous MoSi nanobelts

Qi Chen,[1,*] Biao Zhang,[1,*] La-bao Zhang,[1,†] Fei-yan Li,[1] Fei-fei Jin,[1] Hang Han,[1] Rui Ge,[1] Guang-long He,[1] Hao-chen Li,[1] Jing-rou Tan,[1] Xiao-han Wang,[1] Hao Wang,[1] Shun-li Yu,[2] Xiao-qing Jia,[1] Qing-yuan Zhao,[1] Xue-cou Tu,[1] Lin Kang,[1] Jian Chen,[1] and Pei-heng Wu[1]

[1]*Research Institute of Superconductor Electronics, Nanjing University, No. 163 Xianlin Road, Nanjing 210023, China*
[2]*School of Physics, Nanjing University, No. 163 Xianlin Road, Nanjing 210023, China*

(Received 24 September 2021; revised 17 December 2021; accepted 19 January 2022; published 31 January 2022)

A traditional concept proposes that the suppression of the transition temperature T_c in an amorphous nanobelt is driven by enhanced disorder, which accounts for localized Cooper pairs. However, in this paper, we observe T_c suppression in an amorphous molybdenum-silicide (MoSi) nanobelt, which scales as the inverse square of the width but contradicts disorder theory. Instead, the transition regime can be well described by Cooper pair diffusion in the proximity effect. Both the nonlinear reduction of the switching current density and the abnormal increase of the effective retrapping current density with the reduction of the width further verify the proximity-induced relation. Therefore, we attribute the main size dependence of the suppressed superconducting properties in the MoSi nanobelt to the proximity effect rather than disorder. We speculate that the competition between superconductivity and disorder only appears at the two narrow edge bands rather than the entire nanobelt. Subsequently, the reduction in width does not produce a significant impact on superconductivity for disorder, and only the proximity effect plays an overwhelming role in the MoSi nanobelt.

DOI: 10.1103/PhysRevB.105.014516

I. INTRODUCTION

Exploiting superconductivity in low-dimensional structures is of great significance to the fundamental research of superconducting physics and the development of advanced low-dimensional superconducting devices. Superconductor properties (such as critical transition temperature T_c and switching current density j_{SW}) will change significantly in structures where the size is reduced comparable to or smaller than the superconducting coherence length ξ and magnetic field penetration depth λ. How small can superconductors be? The Anderson criterion suggests that there is the smallest size at which the Kubo gap (mean electronic energy level spacing near the Fermi energy) exceeds the bulk, zero-temperature superconducting energy gap [1]. It has been experimentally validated in many zero-dimensional isolated grains or compacted powders, such as Nb [2] and Pb [3] nanoparticles.

When a superconductor is patterned into a nanobelt with a certain width w, the variation in w also influences the superconductivity of the nanobelt. It has previously been shown that T_c can be affected significantly by disorder in a nanobelt [4–9]. Upon increasing disorder, the suppression of T_c toward zero occurs due to the competition between the enhanced Coulomb repulsion and the Cooper pairing.

Recently, a novel promising amorphous film, MoSi, has been the subject of numerous experimental and theoretical research studies [10–13] due to various advantages, such as lenient substrate requirements and lower superconducting energy gap. For example, it has been widely developed into superconducting nanowire single photon detectors (SNSPDs), exhibiting excellent detection metrics in the near infrared band [14], which enables SNSPDs to have great potential in scientific applications such as long-distance quantum teleportation [15]. A new record system detection efficiency (SDE) of $98.0 \pm 0.5\%$ at the wavelength of 1550 nm was achieved based on high-quality MoSi film [13]. Besides, SNSPD made of thin MoSi film with awidth of micrometers and an active area up to $10^5\ \mu m^2$ can also obtain saturated internal detection efficiency (IDE) at a 1550 nm wavelength [11]. Furthermore, a saturated IDE at an $\sim 5\ \mu$m wavelength for 30 nm wide meander-shaped MoSi SNSPD was also demonstrated [16].

The study of the superconductivity in MoSi nanostructures, such as the nanobelt, which have the possibility of tuning their superconducting state by changing their width, is of fundamental interest. In this paper, we have studied the superconducting properties of $Mo_{0.8}Si_{0.2}$ nanobelts. However, we observed that the nanobelts undergo T_c suppression, which is linearly related to $1/w^2$ and is inconsistent with disorder predictions.

II. METHODS

In the experiment, $Mo_{0.8}Si_{0.2}$ was chosen as the material, and 11 sets of samples were prepared on a single chip to ensure that all the $Mo_{0.8}Si_{0.2}$ nanobelts with different widths could have the same thickness. Furthermore, all the nanobelts have the same length of 20 μm, and the width w is distributed between 30 nm and 3 μm. In addition, the area between the nanobelts and the contact pads is designed to be an arc-angle structure to effectively avoid current crowding [17].

The fabrication method can be found in our previous work [16]. The 5 nm thick $Mo_{0.8}Si_{0.2}$ film is deposited using current-controlled DC magnetron sputtering of a $Mo_{0.8}Si_{0.2}$

*These authors contributed equally to this work.
†Corresponding author: lzhang@nju.edu.cn

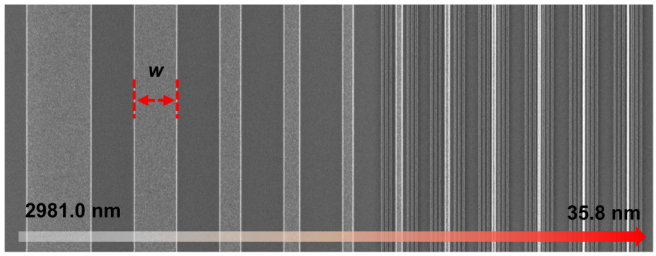

FIG. 1. SEM image of the $Mo_{0.8}Si_{0.2}$ nanobelts, which are prepared by negative lithography over HSQ resist. The widths are decreased from 2981.0 to 35.8 nm, as shown by the red arrow. The dark wires near the narrow nanobelts act as the dose correctors during the EBL process.

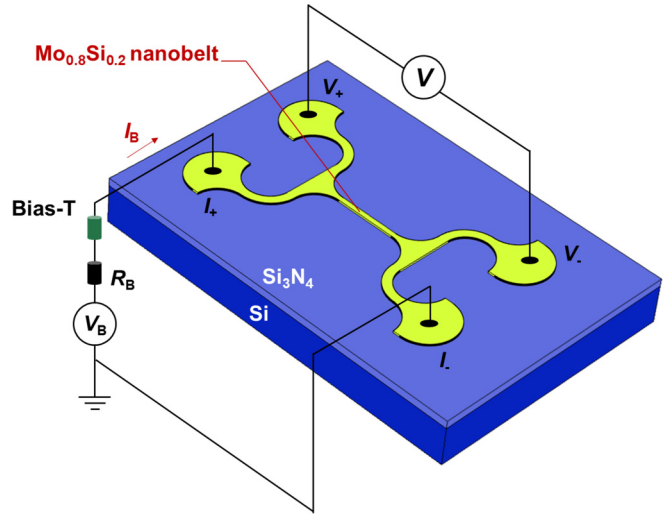

FIG. 2. Schematic describing the measurement configuration of the $Mo_{0.8}Si_{0.2}$ nanobelt.

alloy target in Ar plasma on a thermal nitride silicon wafer (Si/Si_3N_4) at room temperature (23 °C). A 3 nm thick Nb_5N_6 capping layer is then deposited on the $Mo_{0.8}Si_{0.2}$ film surface using rf magnetron sputtering to avoid oxidation of the $Mo_{0.8}Si_{0.2}$ film. Hydrogen silsesquioxane (HSQ) with a solute concentration of 2% is adopted to coat the $Mo_{0.8}Si_{0.2}$ film. Then the HSQ coating was prebaked at 90 °C for 4 min. After the electron beam exposure (EBL) process, the chip was baked at 90 °C for 2 min, and then the chip was developed in the 2.38% TMAH developer at room temperature (23 °C) for 3 min. The nanopatterns were transferred to the $Mo_{0.8}Si_{0.2}$ film by the reactive ion etching (RIE) process. The etching parameters used in the experiment are as follows: SF_6 and CHF_3 gases with flow rates of 40 and 20 SCCM (cubic centimeters per minute at STP), respectively, the pressure of 4 Pa, the power of 80 W, and the etching time of 27 s. The scanning electron microscope (SEM) image of the $Mo_{0.8}Si_{0.2}$ nanobelts is shown in Fig. 1, and the width ranges from 2981.0 to 35.8 nm.

The current/voltage input ports between the nanobelts are independent of each other, and all the current/voltage output ports share the same ground. The temperature-dependent resistances for all nanobelts are measured by the four-probe technique. To avoid heating- or current-induced vortex motion, the bias current is set to be less than 1/20 of the switching current of each nanobelt. The critical transition temperature is defined as the temperature corresponding to the resistance equal to $0.1R_n$ (R_n is the normal resistance of the nanobelt at 10 K) [18,19]. The critical transition temperature T_{c0} of the $Mo_{0.8}Si_{0.2}$ film is measured to be 4.12 K. We measured the transport characteristics of each nanobelt based on the schematic shown in Fig. 2. The adjustable voltage source (Keithley 2400) V_B and the current limiting resistor R_B (100 kΩ) together provide a variable bias current I_B to the nanobelt. The bias current flows into the nanobelt through the rf and DC terminal of the bias-T. The rf port of the bias-T is connected to a load cap with resist $R_0 = 50\,\Omega$ to prevent the bridge from entering a stable self-heating state.

III. RESULTS AND DISCUSSION

A. T_c characteristics

It is generally considered that decreasing w leads to increased disorder and further T_c suppression. The relevant characteristic length for superconductivity in the presence of disorder is the thermal diffusion length $L_T = [hD/(2\pi k_B T)]^{0.5}$, where h is the Planck constant, D is the electron diffusion constant, k_B is the Boltzmann constant, and T is the operating temperature. The one-dimensional approximation is valid if w is smaller than L_T. Previous reports in the literature have theoretically proposed that the relative suppression of T_c varies as $1/w$ in two-dimensional superconducting films [20], while the T_c of one-dimensional superconducting wires decreases exponentially with the inverse of the wire cross section [7]. However, in this experiment, the linear relationship between T_c and $1/w^2$ is found in the $Mo_{0.8}Si_{0.2}$ nanobelts, as shown in Fig. 3(a). Strikingly, it differs from the theoretical models mentioned above. $L_T \approx 11.2$ nm at 3 K is calculated for the $Mo_{0.8}Si_{0.2}$ films with a D of $0.49\,cm^2/s$. Thus, all the $Mo_{0.8}Si_{0.2}$ nanobelts are not in the one-dimensional limit. Although Graybeal *et al.* [4] suggested that the observed w^{-2} behavior of T_c is characteristic of the crossover from two dimensional to one dimensional, further accurate efforts are required to resolve how T_c is affected by w in this paper.

B. Proximity effect model

It is well understood that disorder-induced enhancement of the Coulomb interaction inherently competes with superconductivity. As a result, the weaker the attraction in Cooper pairs is, the lower the transition temperature T_c will be. In our work, we speculate that the cross section of the nanobelt can approximately consist of a normal-superconducting-normal (NSN) structure, as shown in Fig. 3(b). The competition between superconductivity and disorder only occurs at the two edge bands of the nanobelt and can strongly reduce the superconducting order parameter Ψ, which finally suppresses the T_c of the edge bands. The width of a single normal edge band is defined as $w_n/2$, and we assume that $w_n/2$ is independent of the nanobelt width. The strong disorder in the two edge bands may be caused by two main factors. One is the bombardment of the edges by high-energy S or F atoms during

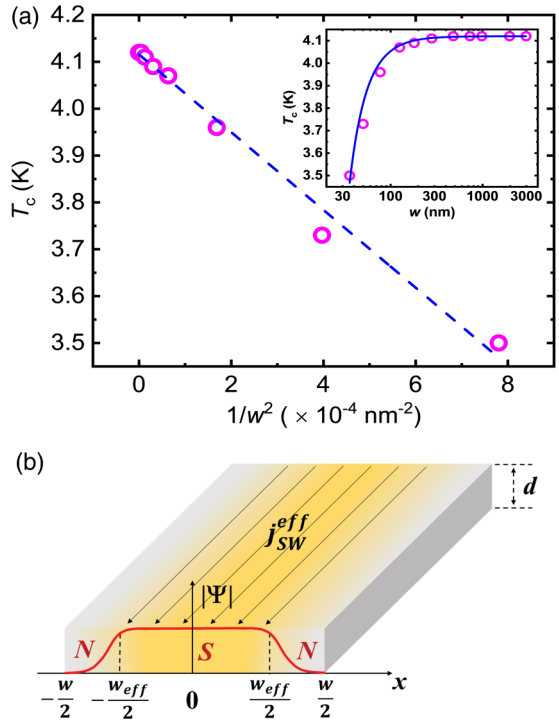

FIG. 3. (a) The T_c of $Mo_{0.8}Si_{0.2}$ nanobelts versus $1/w^2$; the dark blue dashed line indicates the linear relationship between these data. T_c versus w is also shown in the inset, and the dark blue solid line in the inset is calculated by Eq. (1). (b) The normal-superconducting-normal (NSN) structure of the $Mo_{0.8}Si_{0.2}$ nanobelt, where $w_{\rm eff}$ and d are defined as the effective width and the thickness, respectively. The orange gradient color represents the change in the superconducting order parameter Ψ, and Ψ distributes homogeneously in the central superconducting band. $j_{\rm SW}^{\rm eff}$ is the local effective switching current density in the central superconducting band.

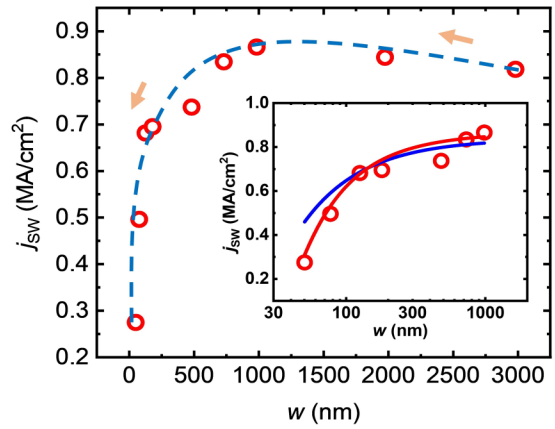

FIG. 4. Dependence of the switching current density $j_{\rm SW}$ on the width of the $Mo_{0.8}Si_{0.2}$ nanobelts. The orange arrows indicate the trend of $j_{\rm SW}$, and the blue dashed line guides the eyes. The inset zooms in on the interval $w < 983.3$ nm. The standard deviation of all the measured values is less than 10%.

the reactive ion etching (RIE) process because the side walls of the nanobelt are not well protected by resist. Another is the oxidation of the side walls when they are exposed to air, and partial oxidation suppresses the superconductivity of the edge bands. Thus, the components in the edge bands will be more complex. On the one hand, both Mo and Si will react with other alien atoms; on the other hand, the value x of Mo_xSi_{1-x} will make a difference. For example, Mo_xSi_{1-x} recrystallization primarily occurs at low Si content ($x \geqslant 0.8$) [21], and the Mo_3Si structure ($T_c = 1.3$ K for bulk superconductor) will be easy to form according to Ref. [22]. Thus, there exists an overwhelming mechanism caused by the diffusion behavior of Cooper pairs, named the proximity effect. The proximity effect between the two edge bands and the central superconducting band would systematically suppress the superconductivity of the whole nanobelt according to Cooper's estimation [23] because of the NSN structure.

We followed the theoretical model used by Liniger based on the nonlinear Ginzburg-Landau (GL) equation [24]. The model shows that Ψ vanishes if the size of the superconducting slab is less than a critical value S_c, where $S_c = 2\xi(T)\arctan[\xi(T)/b]$ and b defines the extrapolation length, which measures the depth of penetration of Cooper pairs into the normal metal region. Here, b tends to be zero due to the strong proximity effect. Therefore, we obtained a critical width of $w_c \approx \pi\xi(T)$, where $\xi(T)$ is the temperature-dependent superconducting coherence length of the $Mo_{0.8}Si_{0.2}$ thin film and $\xi(T) = \xi(0)(1-T/T_{c0})^{-0.5}(1+T/T_{c0})^{-0.25}$ in the full-temperature range, where T_{c0} is measured to be 4.12 K. We then express the transition temperature T_c dependence of the width w by simplifying the analysis in the limit of T_c near T_{c0}:

$$\frac{T_c}{T_{c0}} = 1 - \frac{1}{\sqrt{2}}\left[\frac{\pi\xi(0)}{w - w_n}\right]^2, \tag{1}$$

where $\xi(0)$ of the $Mo_{0.8}Si_{0.2}$ film is approximately 4.5 nm [25], $w_{\rm n}$ is defined as the only fitting parameter, and $w_{\rm n}$ can be obtained to be ~6 nm from the best fitting. This means that the change in transition temperature is approximately proportional to the inverse square of the width ($1/w^2$) according to Eq. (1), which demonstrates the linear relationship between T_c and $1/w^2$ that we observed earlier. The inset of Fig. 3(a) shows the relationship between T_c and w more clearly. Typically, for nanobelts wider than 180.4 nm, the T_c is independent of the width and shows a plateau behavior. For narrower nanobelts, a significant reduction in T_c is observed. The experimental results are well described by Eq. (1), as shown by the blue solid curve.

C. Current density characteristics

The square resistance of the $Mo_{0.8}Si_{0.2}$ film at room temperature is $R_{\rm sq} = 289.3\Omega/{\rm sq}$, so the room temperature resistivity $\rho_{\rm n}$ can be calculated as $\rho_{\rm n} = R_{\rm sq}d = 144.7\,\mu\Omega\,{\rm cm}$. The magnetic field penetration depth $\lambda = 2\lambda_0/d$, where $\lambda_0 = (\hbar\rho_{\rm n}/\mu_0\pi\Delta_0)^{0.5}$; μ_0 is the permeability of vacuum, Δ_0 is the superconducting energy gap at 0 K, and $\Delta_0 = 1.764\,k_BT_c$. Here, λ is calculated to be 154.8 μm, much larger than the width of all measured nanobelts. Thus, it can be seen that the supercurrent distributes homogeneously over the superconducting band of the nanobelt.

Figure 4 shows the switching current density $j_{\rm SW}$ of the nanobelts under the condition of $T = 3.2$ K. The maximum

value of $j_{SW} < 1\,MA/cm^2$ for all nanobelts. There is a nonlinear relationship between j_{SW} and w, which can be divided into two cases: (1) j_{SW} slightly decreases with increasing w if $w \geqslant 983.3\,nm$; (2) j_{SW} decreases sharply with decreasing w if $w < 983.3\,nm$. For case 1, the depairing current density j_{depair} of the nanobelt is calculated to be $\sim 1.06\,MA/cm^2$. The depinning current density j_{depin} should be much smaller than the depairing current density j_{depair} according to Ref. [26]. We have estimated j_{depin} to be 10^{-2}–$10^{-3}\,MA/cm^2$ at 3.2 K, which is about two or three orders of magnitude lower than j_{dep}. However, the measured values of j_{SW} distribute between 0.8 and $0.9\,MA/cm^2$. The most likely mechanism is the penetration and movement of vortices according to the three-current model proposed by Il'in *et al.* [27]. The detailed exploration is under discussion in our future work.

For case 2, we can conclude that j_{SW} has a temperature-dependent relation based on proximity effect:

$$j_{SW}(t) = j_{SW}^{eff}(t)\frac{w_{eff}}{w}, \tag{2}$$

where $t = T/T_c$ and $j_{SW}^{eff}(t)$ is the local effective switching current density in the central superconducting band. As shown in Fig. 3(b), the size of the unstable mode of the superconducting order parameter Ψ from the central superconducting band to the normal edge band is on the order of the temperature-dependent superconducting coherence length of the nanobelt $\xi_0(t)$ [28]. Thus, the effective width w_{eff} can be estimated, $w_{eff} \approx w - w_n - 2\xi_0(t)$. First, we set $j_{SW}^{eff}(t)$ as a constant fitting factor independent of w [29]. The fitting result is shown by the dark blue solid line in the inset of Fig. 4. However, the theoretical prediction deviates slightly from the experimental results. This is because the reduction of w can suppress T_c, which in turn affects $j_{SW}^{eff}(t)$. We build the relationship between $j_{SW}^{eff}(t)$ and w based on the KL model [30]:

$$j_{SW}^{eff}(t) = j_{SW}^{eff}(0)\frac{p_d(t)}{p_d(0)}\frac{\lambda^2(0)\xi(0)}{\lambda_0{}^2(t)\xi_0(t)}, \tag{3}$$

where $j_{SW}^{eff}(0)$ defines the maximum effective switching current density that can be measured at 0 K, $p_d(t)$ is a nondimensional calibration factor, $\xi_0(t) = \xi(0)(1-t)^{-0.5}(1+t)^{-0.25}$. $\lambda_0(t)$ is the magnetic field penetration depth, $\lambda_0(t) = \lambda(0)(1-t^2)^{-0.5}(1+t^{1.5})^{-0.25}$. The experimental results can be well described by the refined relation when setting $j_{SW}^{eff}(0)$ as the only fitting factor, as shown by the red solid line in the inset of Fig. 4. As a result, the fitting factor $j_{SW}^{eff}(0)$ is $3.65\,MA/cm^2$.

To further study $j_{SW}^{eff}(t)$, several samples with different widths are measured (Fig. 5). $j_{SW}^{eff}(t)$ approaches the theoretical value predicted by the KL model; if t tends to 1, it deviates from the theoretical value as t decreases. $j_{SW}^{eff}(t)$ increases monotonically with decreasing temperature and finally tends to saturate at each w. It can be estimated that the maximum value of $j_{SW}^{eff}(0)$ is about $3.79\,MA/cm^2$, close to the best fitting result of $3.65\,MA/cm^2$. Furthermore, we find that $j_{SW}^{eff}(t)$ varies nonmonotonically with the width at different temperatures. We speculate that this can be caused by several reasons: (i) The reduction behavior of w can suppress T_c and then suppress the value of j_{SW}^{eff} as we discussed above; (ii) there is a competition between the magnetic vortex motion and the phase slip. The density of the transport current required

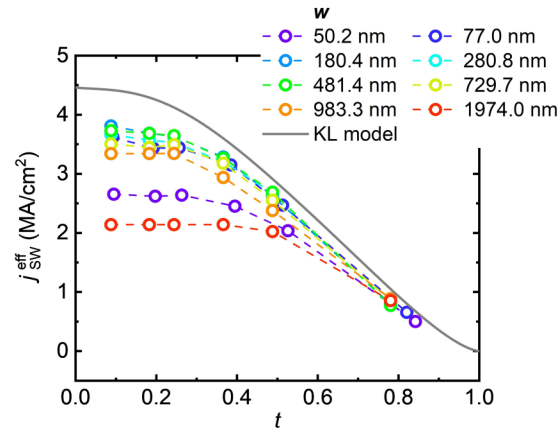

FIG. 5. Dependence of j_{SW}^{eff} on the temperature. There are several samples with different widths, and the gray solid line represents the theoretical value calculated by the KL model. The standard deviation of all the measured values is less than 10%.

for penetration of magnetic vortices into the wide superconducting nanobelt can be proportional to $w^{-2.5}\ln[2w/(\pi\xi)]$, which results in the reduction of w with the increase in j_{SW}^{eff}. However, the phase slip energy barrier is proportional to w [31]. Thus, as w decreases, the phase slip rate will increase exponentially, which severely suppresses the value of j_{SW}^{eff}.

In addition, we observed an abnormal nonlinear relationship between the effective retrapping current density j_r^{eff} and the effective width w_{eff} ($j_r^{eff} = j_r(w/w_{eff})$, where j_r is the measured retrapping current density and $w_{eff} = w - w_c$). Figure 6(a) shows that j_r^{eff} gradually increases with decreasing w_{eff} and rapidly increases if $w_{eff} < 300\,nm$.

The quantitative analysis is still under discussion. However, one possible reason is the self-heating mechanism. That is, there is a thermal diffusion length L_T and a thermal volume V_T in the substrate as discussed in Ref. [32]. For a superconducting nanobelt with an effective width $w_{eff} < L_T$, V_T will decrease slower than the nanobelt volume when w_{eff} decreases. Under this condition, the narrower nanobelt will be much better refrigerated by the substrate than the wider one. Here we conduct a simple analysis based on the two-dimensional self-heating model. Regardless of the time evolution of the nanobelt temperature at the effective retrapping current density j_r^{eff} the relationship between w_{eff} and j_r^{eff} can be estimated to be $1/w_{eff} \propto j_r^{eff}(j_r^{eff}/j_{SW}^{eff} - 1)^n$, where n is a temperature-dependent free parameter and $(j_r^{eff}/j_{SW}^{eff} - 1)^n$ increases exponentially with the j_r^{eff} increase. Thus, the abnormally increasing behavior of j_r^{eff} as w_{eff} decreases can get a qualitative explanation in view of the estimation above.

Another possible reason is the lateral thermal diffusion behavior due to the proximity effect in the nanobelts, as discussed before [29]. When the nanobelts transit from the superconducting state to the normal state, the temperature in the central band is much higher than that in the adjacent normal edge bands due to Joule heating because most of the supercurrent is concentrated in the central band (has a width of w_{eff} approximately). Therefore, there is an extra lateral thermal diffusion channel where heat flows from the center

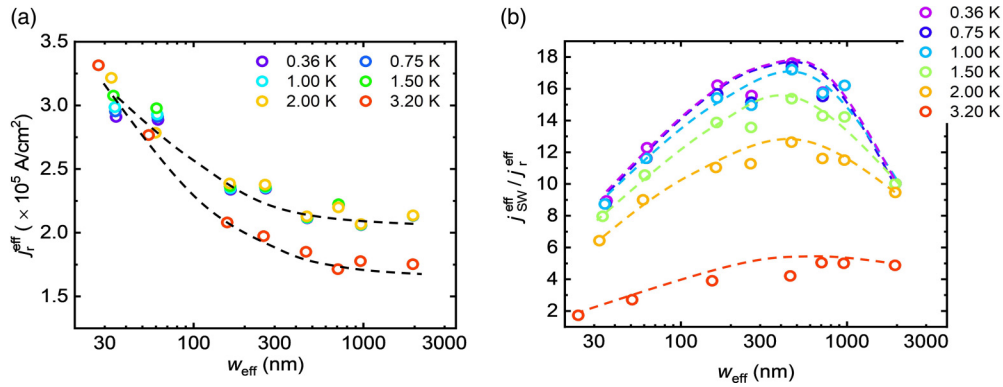

FIG. 6. (a) Dependence of the effective retrapping current density j_r^{eff} on the efficient width w_{eff} under different temperature environments. (b) Dependence of the ratio between j_{SW}^{eff} and j_r^{eff} on w_{eff} under different temperature environments. All the dashed lines in (a,b) are to guide the eyes. The standard deviation of all the measured values is less than 5%.

band to the edge bands in addition to along the nanobelt and toward the substrate. The thermal diffusion radius $r = (D\tau_D)^{0.5}$, where τ_D is the electron relaxation time. If $w_{eff} > 2r$, the lateral thermal diffusion could be negligible. However, if $w_{eff} \leqslant 2r$, the lateral thermal diffusion will accelerate the cooling rate, making j_r^{eff} keep rising. The τ_D of amorphous superconducting materials was measured to be hundreds of picoseconds [33]. Therefore, $2r$ is distributed between 140 and 450 nm, which is basically in line with the experimental result of about 300 nm. Furthermore, the reduction behavior of j_r^{eff} at the same w_{eff} is consistent with the model proposed by Stockhausen *et al.* [34] if T approaches T_c. However, the j_r^{eff} will be temperature independent if w_{eff} decreases below 30 nm, resulting from the enhanced lateral thermal diffusion effect in the ultranarrow nanobelts.

We further studied the ratio of j_{SW}^{eff} to j_r^{eff} as a function of w_{eff} and T, as shown in Fig. 6(b). The ratio changes with the w_{eff} in a "Λ" shape. In addition, the ratio increases with decreasing T and tends to saturate below 1 K. The w_{eff} stays at about 500 nm, where the ratio can achieve the peak value. In addition, the "Λ" shape becomes flatter as T increases. The results can provide suitable guidance for the design of a single photon detector such as SNSPD. If the nanowire width remains unchanged, the higher the ratio is, the better the detection performance [35]. We can see that the MoSi nanobelts will reach a saturated ratio if the temperature is below 1 K. This will give us a revelation: The detection performances of MoSi SNSPD operated at temperatures approaching 1 K or tens of mK will be almost the same. Thus, the cooling demand for SNSPDs (especially for midinfrared SNSPDs) can be decreased. For example, the midinfrared SNSPD does not always have to work at temperatures lower than 0.3 K; instead, it shows saturated internal detection efficiency up to a wavelength of 10 μm at 0.85 K [36].

Finally, we found that similar phenomena can appear in both amorphous and polycrystalline superconducting materials when comparing our work with the work of Charaev *et al.* [29]. For example, similar dependences of both T_c and j_{SW} at the measured temperature on w are observed. Thus, we speculate that the proximity effect induced by Cooper pair diffusion may be another universal physical mechanism in low-dimensional superconductors in addition to disorder. More specifically, however, we find that the effective switching current density in the central superconducting band varies nonmonotonically with the width of the $Mo_{0.8}Si_{0.2}$ nanobelt over the whole range of temperatures, which differs from the monotonical increase behavior of NbN at 4.2 K. The nonlinear relationship can be caused by T_c suppression and the competition between the magnetic vortex motion and the phase slip as we have discussed above. We believe that the results in this paper will provide a valuable reference for the design of high-performance photon detectors based on MoSi.

IV. CONCLUSION

In summary, we have studied the superconducting transport properties of $Mo_{0.8}Si_{0.2}$ nanobelts. We observe that these nanobelts undergo a strong and systematic reduction in T_c with decreasing w, and the T_c is linearly related to w^{-2}. This result is not consistent with a process driven by disorder. However, it can be well described by the Cooper pair diffusion induced proximity effect. Furthermore, the nonlinear evolutions of j_{SW} and j_r^{eff} under the condition of width reduction are also observed, which can well verify the proximity-induced relation. We attribute the main size dependence of the suppressed superconducting properties in the MoSi nanobelt to the proximity effect rather than disorder.

ACKNOWLEDGMENTS

This work is supported by the National Natural Science Foundation of China (Grants No. 12033002, No. 61521001, No. 62071218, No. 62071214, No. 61801206, No. 11227904, and No. 12074175), the National Key R&D Program of China (Grant No. 2017YFA0304002), Key-Area Research and Development Program of Guangdong Province (Grant No. 2020B0303020001), the Fundamental Research Funds for the Central Universities, the Priority Academic Program Development of Jiangsu Higher Education Institutions (PAPD), the Recruitment Program for Young Professionals, the Qing Lan Project, and the Jiangsu Provincial Key Laboratory of Advanced Manipulating Technique of Electromagnetic Waves.

[1] P. W. Anderson, J. Phys. Chem. Solids **11**, 26 (1959).
[2] S. Bose, P. Raychaudhuri, R. Banerjee, P. Vasa, and P. Ayyub, Phys. Rev. Lett. **95**, 147003 (2005).
[3] S. Vlaic, S. Pons, T. Zhang, A. Assouline, A. Zimmers, C. David, and S. Vlaic, Nat. Commun. **8**, 14549 (2017).
[4] J. M. Graybeal, P. M. Mankiewich, R. C. Dynes, and M. R. Beasley, Phys. Rev. Lett. **59**, 2697 (1987).
[5] Y. Oreg and A. M. Finkel'stein, Phys. Rev. Lett. **83**, 191 (1999).
[6] J. M. Graybeal and M. R. Beasley, Phys. Rev. B **29**, 4167(R) (1984).
[7] H. Kim, S. Jamali, and A. Rogachev, Phys. Rev. Lett. **109**, 027002 (2012).
[8] F. Sharifi, A. V. Herzog, and R. C. Dynes, Phys. Rev. Lett. **71**, 428 (1993).
[9] T. R. Kirkpatrick and D. Belitz, Phys. Rev. Lett. **68**, 3232 (1992).
[10] V. B. Verma, B. Korzh, F. Bussières, R. D. Horansky, S. D. Dyer, A. E. Lita, F. Marsili, M. D. Shaw, H. Zbinden, R. P. Mirin, and S. W. Nam, Opt. Express **23**, 33792 (2015).
[11] I. Charaev, Y. Morimoto, A. Dane, A. Agarwal, M. Colangelo, and K. K. Berggren, Appl. Phys. Lett. **116**, 242603 (2020).
[12] A. Banerjee, L. J. Baker, A. Doye, and M. Nord, Supercond. Sci. Technol. **30**, 084010 (2017).
[13] D. V. Reddy, R. R. Nerem, S. W. Nam, R. P. Mirin, and V. B. Verma, Optica **7**, 1649 (2020).
[14] F. Li, H. Han, Q. Chen, B. Zhang, H. Bao, Y. Dai, R. Ge, S. Guo, G. He, Y. Fei, S. Yang, X. Wang, H. Wang, X. Jia, Q. Zhao, L. Zhang, L. Kang, and P. Wu, Photon. Res. **9**, 389 (2021).
[15] H. Takesue, D. D. Shellee, J. S. Martin, V. Verma, R. P. Mirin, and S. W. Nam, Optica **2**, 832 (2015).
[16] Q. Chen, R. Ge, L. Zhang, F. Li, B. Zhang, F. Jin, H. Han, Y. Dai, G. He, Y. Fei, X. Wang, H. Wang, X. Jia, Q. Zhao, X. Tu, L. Kang, J. Chen, and P. Wu, Sci. Bull. **66**, 965 (2021).
[17] H. L. Hortensius, E. F. C. Driessen, T. M. Klapwijk, K. K. Berggren, and J. R. Clem, Appl. Phys. Lett. **100**, 182602 (2012).
[18] N. Hadacek, M. Sanquer, and J. C. Villegier, Phys. Rev. B **69**, 024505 (2004).
[19] J. E. Sadleir, S. J. Smith, I. K. Robinson, F. M. Finkbeiner, J. A. Chervenak, S. R. Bandler, M. E. Eckart, and C. A. Kilbourne, Phys. Rev. B **84**, 184502 (2011).
[20] R. A. Smith, B. S. Handy, and V. Ambegaokar, Phys. Rev. B **63**, 094513 (2001).
[21] B. Krause, G. Abadias, A. Michel, P. Wochner, S. Ibrahimkutty, and T. Baumbach, ACS Appl. Mater. Interfaces **8**, 34888 (2016).
[22] A. E. Lita, V. B. Verma, J. Chiles, and R. P. Mirin, Supercond. Sci. Technol. **34**, 054001 (2021).
[23] L. N. Cooper, Phys. Rev. Lett. **6**, 689 (1961).
[24] W. Liniger, J. Low Temp. Phys. **93**, 1 (1993).
[25] S. Kubo, J. Appl. Phys. **63**, 2033 (1988).
[26] K. K. Likharev, Rev. Mod. Phys. **51**, 101 (1979).
[27] K. Il'in, M. Siegel, A. Engel, H. Bartolf, A. Schilling, A. Semenov, and H.-W. Huebers, J. Low Temp. Phys. **151**, 585 (2008).
[28] M. Serbyn and M. A. Skvortsov, Phys. Rev. B **87**, 020501(R) (2013).
[29] I. Charaev, T. Silbernagel, B. Bachowsky, A. Kuzmin, S. Doerner, K. Ilin, A. Semenov, D. Roditchev, D. Y. Vodolazov, and M. Siegel, Phys. Rev. B **96**, 184517 (2017).
[30] J. R. Clem and V. G. Kogan, Phys. Rev. B **86**, 174521 (2012).
[31] B. Pannetier, J. Villegier, and V. Bouchiat, Nano Lett. **12**, 3501 (2012).
[32] M. Ruibal, G. Ferro, M. R. Osorio, J. Maza, J. A. Veira, and F. Vidal, Phys. Rev. B **75**, 012504 (2007).
[33] F. Marsili, M. J. Stevens, A. Kozorezov, V. B. Verma, C. Lambert, J. A. Stern, R. D. Horansky, S. Dyer, S. Duff, D. P. Pappas, A. E. Lita, M. D. Shaw, R. P. Mirin, and S. W. Nam, Phys. Rev. B **93**, 094518 (2016).
[34] A. Stockhausen, K. Il'in, M Siegel, U. Södervall, P. Jedrasik, A. Semenov, and H.-W. Hübers, Supercond. Sci. Technol. **25**, 035012 (2012).
[35] S. Steinhauer, L. Yang, S. Gyger, T. Lettner, C. Errando-Herranz, K. D. Jöns, M. A. Baghban, K. Gallo, J. Zichi, and V. Zwiller, Appl. Phys. Lett. **116**, 171101 (2020).
[36] V. B. Verma, E. E. Wollman, K. K. Berggren, B. Korzh, A. B. Walter, A. D. Beyer, J. P. Allmaras, R. P. Mirin, S. W. Nam, A. E. Lita, R. M. Briggs, M. Colangelo, Y. Zhai, H. Vora, D. Zhu, E. Schmidt, A. G. Kozorezov, and M. D. Shaw, APL Photon. **6**, 056101 (2021).